MDPI

*Article*

# Vegetation Changes and Dynamics of the Climate Variables in Southern Thailand over the Past 1500 Years

Jian Wang [1], Lijuan Sha [1,*], Jin He [1], Xinnan Zhao [2,*], Rui Zhang [1], Baojun Yang [3] and Hai Cheng [1,4]

1   Institute of Global Environmental Change, Xi'an Jiaotong University, Xi'an 712000, China;
    wang1231@stu.xjtu.edu.cn (J.W.)
2   School of Geography and Tourism, Huizhou University, Huizhou 516007, China
3   Pridi Banongrong International College, Thammasat University, Bangkok 10200, Thailand
4   State Key Laboratory of Loess and Quaternary Geology, Institute of Earth Environment, Chinese Academy of
    Sciences, Xi'an 710061, China
*   Correspondence: shalijuan@xjtu.edu.cn (L.S.); zhaoxinnan@hzu.edu.cn (X.Z.)

**Abstract:** The Indo-Pacific, a vast biogeographic of Earth, is influenced by both the Indian and East Asian monsoons. Despite its geographical importance, this region has been less studied compared to East Asia and India. Here, we present speleothem records from southern Thailand that cover the last 1500 years, including a hiatus during the Little Ice Age, providing insights into the interactions among climate dynamics, human influences, and ecological responses to climate change. Notably, our records lack the characteristic cold and warm periods observed in other regions, such as the Dark Ages Cold Period and Medieval Warm Period, which may reflect the complexity of the tropical climate system or the region's unique topography. The analysis reveals a link between ENSO multi-decadal variability and hydroclimate conditions in southern Thailand, as evidenced by speleothem $\delta^{18}O$. Furthermore, a comparison between speleothem $\delta^{13}C$ and the Normalized Difference Vegetation Index (NDVI) indicates significant vegetation changes in the last three decades, corresponding with increased atmospheric $CO_2$ levels and expansion of agricultural land due to human activities during the Current Warm Period. Additionally, our study suggests that an abrupt increase in sea surface temperatures may enhance vegetation growth in the Indo-Pacific by influencing atmospheric circulation and increasing precipitation.

**Keywords:** speleothem; ENSO; NDVI; vegetation changes; climate changes

## 1. Introduction

Throughout history, the interaction between the natural environment and its dynamic processes has profoundly influenced human decision-making and the evolution of societies [1–3]. Research dedicated to understanding the characteristics and trends of climate change over the past 2000 years has therefore attracted significant scholarly attention [4,5]. This focus is underscored by its designation as a key initiative by the Intergovernmental Panel on Climate Change (IPCC) and as a priority theme within the international research programs of Past Global Changes (PAGES) and Core Project of the World Climate Research Programme (CLIVAR) [6,7]. Such studies are indispensable for unraveling the complex nexus between human actions and climate evolution, establishing the natural benchmarks for modern and future climate scenarios, and devising predictive models and mitigation strategies for forthcoming climatic shifts [8–10].

Southern Thailand, located in the low-latitude tropical region of the Northern Hemisphere, is markedly influenced by both the Indian Summer Monsoon and the Northwest Pacific Summer Monsoon [11,12]. Enhanced research into climate change within this transitional zone is imperative for advancing our comprehension of the evolution and dynamic mechanisms underlying the monsoon systems [13–15]. Moreover, this location makes the

area especially vulnerable to changes in precipitation patterns driven by monsoon dynamics, resulting in either drought or flood disasters that profoundly impact the livelihoods of the local population, socio-economic development, and ecological balance [12]. On the other hand, it has been observed that the landscape of southern Thailand is predominantly characterized by rice paddy fields, with diminishing patches of remnant forest. Specifically, forest cover decreased from 41.9% in 1961 to 16.3% in 2004, primarily due to the expansion of agricultural land [16]. While numerous studies have focused on the vegetation's response to climate variables like rainfall and temperature, demonstrating varying correlations depending on geographical features, moisture availability, and human-induced changes in land use and cover [17–20], there remains a gap in our understanding of vegetation dynamics and their interaction with climate variability in southern Thailand. The challenge of limited modern instrumental meteorological data and scarce long-term historical climate records hampers our comprehension of precipitation and vegetation changes and mechanisms on a century-to-decadal scale. Utilizing climate proxies with precise dating, such as cave stalagmites and tree rings, for reconstructing the long-term history of regional precipitation and vegetation changes, alongside exploring their underlying mechanisms, emerges as a pivotal approach to addressing these critical scientific inquiries.

Relying on favorable hydrothermal conditions, southern Thailand has developed dense tropical forests and rich karst landforms. Currently, research on past climate and environmental changes in the region mainly focuses on tree rings and cave stalagmites. For example, Tan et al. [11] show that the decades-long drying trend in the North Central Indo-Pacific (NCIP) region is not unique in the context of the region's hydroclimate variability during the last two to three millennia; in fact, the study indicates that NCIP was struck by previous episodes of drier condition, rivaling that of the current drying trend. The results suggest that detecting changes in rainfall due to anthropogenic forcing still remains indistinguishable from natural variability in the northern tropics [11]. Therefore, more climate change reconstruction research in the region during the past 2000 years is essential to comprehensively and scientifically understand the spatiotemporal patterns and regulatory mechanisms of climate change in the region.

Understanding the causes of climatic variability in southern Thailand is essential for characterizing the associated feedback mechanisms, such as changes in oceanic conditions and land cover. Here, we present the $\delta^{18}O$, $\delta^{13}C$, and trace elements records, spanning the past 1500 years, including a hiatus during the Little Ice Age, from a precisely dated new stalagmite sourced from Tham Nhong-Lha Cave in southern Thailand. Combined with Normalized Difference Vegetation Index (NDVI) records in Thailand, together with other well-established climatic records, we elucidate the associated dynamical processes linked to the climate changes that occurred across southern Thailand over the past 1500 years.

## 2. Materials and Methods

### 2.1. Cave Sites and Sampling

Stalagmite TNL3 was collected from Tham Nhong-Lha Cave (99.00° E, 9.10° N, 112 m a.s.l.) (Figure 1), which is located in the Surat Thani Province, southern Thailand [21]. The karstic network of the Tham Nhong-Lha cave developed within the white dolomitic limestones of the Permo-carboniferous age (Figure 1a). The cave is about 1000 m long in total, and the narrowest section is less than 1 m; the narrow cave maintains a relative humidity of 95 to 100% in the tunnels and chambers, which are >100 m from the entrance. Sample TNL3 was ~200 m from the entrance (Figure 1b). Many stalactites and stalagmites developed in the cave, and some mud layers on the floor, which might have been caused by heavy rainfall events. Surat Thani Province is one of the most important natural rubber-producing areas in Thailand, and the land around the adoption site is mainly used for cash crops such as rubber trees.
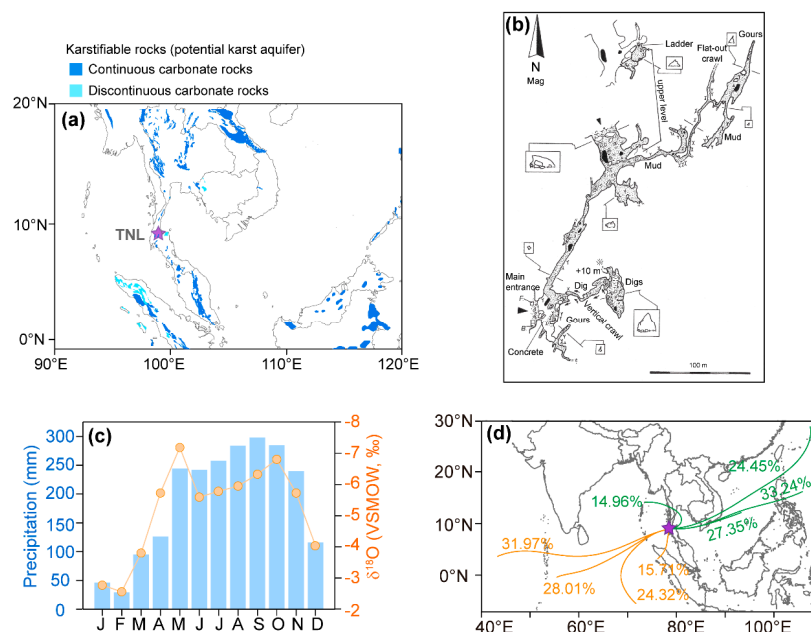
**Figure 1.** Geographic context and modern hydroclimate of the study area. (**a**) Stalagmite TNL3 was collected from Tham Nhong-Lha Cave (99.00° E, 9.10° N, 112 m a.s.l.). The cave site (purple star) is shown on the Global Karst Aquifer Map (WOKAM project: https://www.un-igrac.org/resource/world-karst-aquifer-map-wokam (accessed on 15 November 2023)) [22]. (**b**) The sketch of Tham Nhong-Lha Cave was drawn by M. Laumanns on 21 January 2020. (**c**) Reanalyzed precipitation amount (blue bars) and $\delta^{18}O$ (orange circles connected with orange lines) based on the data (1980–2015) from the National Centers for Environmental Prediction/National Center for Atmospheric Research, NCEP/NCAR (https://www.esrl.noaa.gov (accessed on 15 November 2023)) [23]. (**d**) The bold lines depict the main tracks (labeled with moisture percentages) associated with moisture back-trajectories (120 h, averaged over 2015–2017) for the study area for summer (June–September; yellow) and winter (November–February; green). Back-trajectories were computed using the NOAA HYSPLIT model based on Environmental Prediction/National Center for Atmospheric Research, NCEP/NCAR reanalysis data (https://ready.arl.noaa.gov/HYSPxT_traj.php (accessed on 15 November 2023)) [23].

The southern Thailand (6°~10° N, 97°~102° E) is located in the central part of the Malay Peninsula, which projects into the ocean from the Indo-Pacific [12]. This region experiences a tropical monsoon climate, influenced both by the north-south movements of the Intertropical Convergence Zone (ITCZ) and the characteristics of the tropical monsoon climate itself. The climate of southern Thailand is marked by an annual average temperature of 27.1 °C, with the warmest monthly average temperature peaking at 28.3 °C in April. Conversely, the coolest monthly average temperature is recorded in December, at 26.1 °C. The average annual precipitation is 2390 mm, delineating distinct wet and dry seasons (Figure 1c). The wet season extends from May to November, while the dry season runs from December to April of the subsequent year. Remarkably, rainfall during the wet season contributes to 76% of the annual precipitation, with the summer monsoon (from May to October) providing more than 90% of rainfall, highlighting the significant influence of monsoonal patterns on southern Thailand's climate (Figure 1c).

## 2.2. $^{230}Th$ Dating Method

Stalagmite TNL3 was cut into two sections along the growth axis and then polished. The length of the stalagmite TNL3 was about 360 mm, and its diameter ranged from 30 and 55 mm at the top to 70 mm at the bottom (Figure 2). A total of 16 samples were obtained for $^{230}Th$ dating (Table S1). Dating was performed at the Institute of Global Environmental Change of Xi'an Jiaotong University (China) using a Neptune Plus Multi-

Collector Inductively Coupled Plasma Mass Spectrometer (MC-ICP-MS). The chemical and instrumental procedures were similar to those described in Edwards et al. [24] and Cheng et al. [25]. All ages are reported as two standard deviations (2σ).
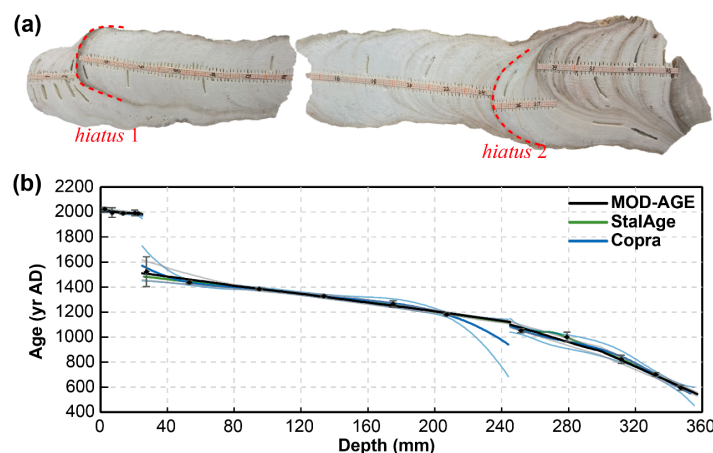


**Figure 2.** Sample profile and age model results. (**a**) Stalagmite TNL3 profile and the dashed lines show 2 hiatuses at depths of 25 and 245 mm. (**b**) the age model results were generated by different software. Diamonds and error bars are U-Th ages. The lines are results with different software, black: MOD-AGE [26], blue: Copra [27], green: StalAge [28], grey and light blue are the 2σ errors of MOD-AGE and Copra, respectively. The results are consistent within the margin of error, and the MOD-AGE result was finally used, taking into account its ability to handle hiatuses.

## 2.3. Stable Isotope and Trace Element Analysis

The subsamples for stable isotope and trace element analysis were drilled by hand using a 0.3 mm diameter drill bit; the average sample interval was 1 mm. The stable isotope composition of the samples was measured by Isotope-Ratio Mass Spectrometry (IRMS) (MAT253 plus) at the Institute of Global Environmental Change of Xi'an Jiaotong University (China). The results (Table S2) are reported relative to the Vienna Pee Dee Belemnite (VPDB) standard with an average 2σ uncertainty of 0.1‰ or less.

The same drilling position powder used for stable isotope analysis was used for trace element analysis. The collected powders were dissolved in 2 mL of 5% $HNO_3$, and the solutions were then prepared for trace element analysis. An inductively coupled plasma optical emission spectrometer (ICP-OES, Agilent 5800, Agilent, Santa Clara, CA, USA) was used to measure element concentrations at the Isotope Laboratory, Xi'an Jiaotong University (China). One in-house standard, BQC, was measured every 10 subsamples, and the standard error of X/Ca is less than 1% (X refers to Sr and Mg) (Table S2).

## 3. Results

### 3.1. Age Models

Stalagmite TNL3 was collected in January 2020 from an active drip site; the stalagmite top thus represents the year 2020 AD, which was further corroborated through [230]Th dating. Together with the 16 [230]Th dates, it is shown that TNL3 spans the interval between ~548 AD and 2020 AD. Two hiatuses were identified with the profile of the TNL3, at depths of 25 and 245 mm (Figure 2).

Age models were constructed using MOD-AGE [26], StalAge [28], and COPRA [27]. The age models were generally consistent with the analytical uncertainties and showed almost the same results (Figure 2b). Therefore, our conclusions are not dependent on the choice of age model. Given the ability to deal with hiatuses, we finally used the age model results from MOD-AGE to construct the time series of proxies (Table S2). The age model results show two hiatuses: between ~1983 and 1510 yr AD and between ~1124 and 1095 yr AD. The final chronology model shows that the 2σ error is less than 20 years at most parts of the stalagmite, thus ensuring that we can discuss climate change in a shorter period.

### 3.2. Interpretation of the Stable Isotope Records

Previous research has highlighted that the dominant moisture source for the rainy season precipitation in southern Thailand, as indicated by precipitation $\delta^{18}O$, primarily originates from proximate water vapor in the Bay of Bengal (Figure 1d). This moisture source is largely governed by convective activities that transport moisture from the source area to southern Thailand and by local precipitation patterns (Figure 1c,d). Moreover, the $\delta^{18}O$ values of precipitation have a negative correlation with precipitation amount (Figure 3c,d). Hence, the $\delta^{18}O$ values of the rainy season precipitation within this region can serve as indicators of local precipitation changes [29].
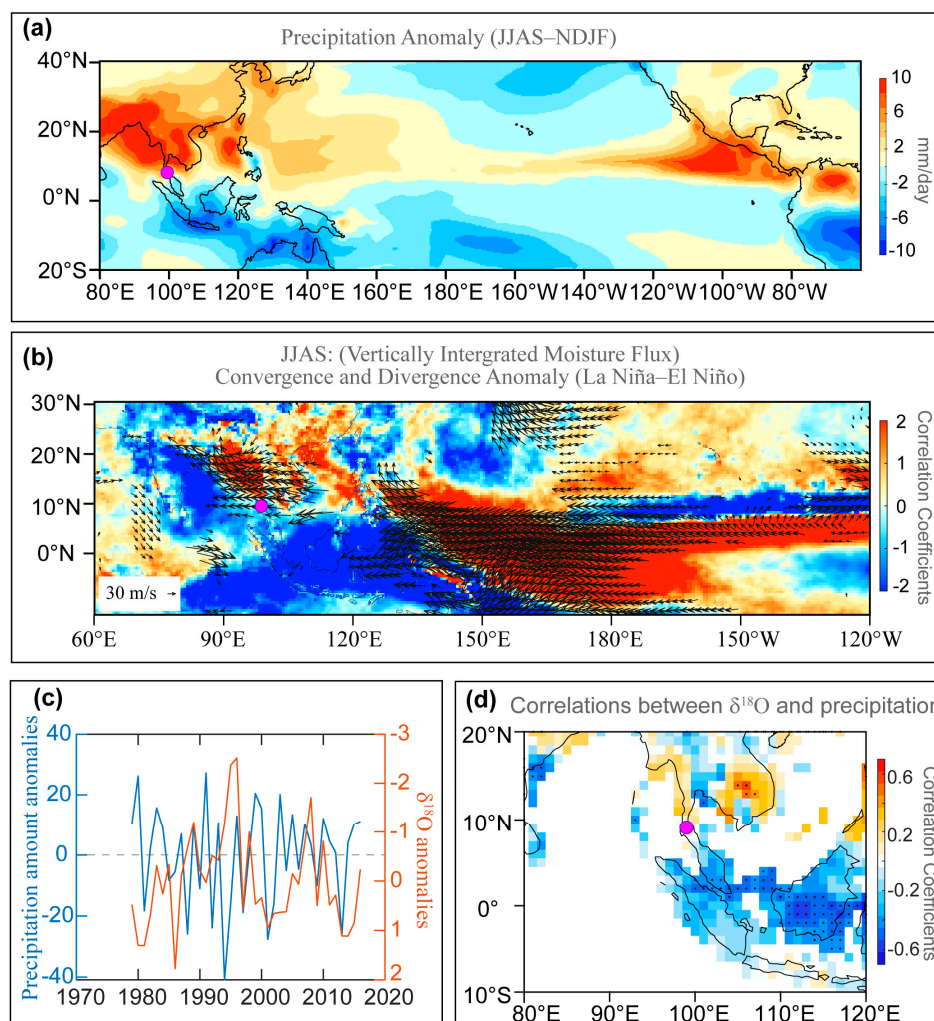


**Figure 3.** Climate setting of the study area. (**a**) Precipitation amount differences between June and September (JJAS) and between November and February (NDJF) in the western Pacific and East Asia (color-scale shown right), based on the data from the Global Precipitation Climatology Project (GPCP) [30]. (**b**) Spatial pattern of the difference in JJAS precipitation (ERA5) between the years marked by El Niño (1982, 1983, 1987, 1992, 1993, 1997, 2006, 2009, and 2012) and La Niña (1988, 1989, 1999, and 2010). (**c**) Monthly mean (JJAS) variations in the anomalies of amount (blue) and amount-weighted $\delta^{18}O_P$ (orange) of precipitation at the cave site over the years 1979–2016. (**d**) The correlation between $\delta^{18}O_P$ of precipitation and precipitation. Reanalyzed precipitation is based on the data (1979–2016) from the National Centers for Environmental Prediction/National Center for Atmospheric Research, NCEP/NCAR (https://www.esrl.noaa.gov (accessed on 15 November 2023)) [23]. The purple circle indicates the location of the Tham Nhong-Lha Cave (99.00° E, 9.10° N, 112m a.s.l.).

While the $\delta^{18}O$ values in speleothems can be influenced by numerous hydroclimatic factors, including temperature, relative humidity, and evaporation, consistent patterns observed across different stalagmite records suggest that $\delta^{18}O$ variability predominantly reflects a common environmental factor. The published $\delta^{18}O$ records from stalagmites in southern Thailand are indicative of shifts in local precipitation $\delta^{18}O$, thus mirroring changes in local precipitation [11]. These variations not only document local precipitation dynamics but also respond to large-scale climatic and environmental changes in the region. This duality underscores the utility of speleothem $\delta^{18}O$ analysis in reconstructing past hydroclimate variations, offering valuable insights into the interplay between local precipitation dynamics and larger-scale environmental conditions (Figure 3d).

On the other hand, speleothem $\delta^{13}C$ records are affected by a range of processes [10,31], including changes in atmospheric $CO_2$ isotopic composition and the degree of mixing between atmospheric $CO_2$ and biological $CO_2$ derived from root respiration and microbial activity [32]; changes in the ratio of C3:C4 plants in the overlying vegetation [33] and vegetation density above the cave [34]; and changes in the amount of prior calcite precipitation (PCP), in the roof of the cave and/or elsewhere in the aquifer system [35], and so on. Given the tropical monsoon climate of southern Thailand, characterized by concurrent rainfall and warmth, we can derive specific insights into speleothem $\delta^{13}C$: (1) During the rainy season or humid climate periods, the region experiences high precipitation and elevated soil $CO_2$ concentrations, leading to negative $\delta^{13}C$ values, a lack of preferential calcium carbonate deposition in the aquifer, and negative $\delta^{13}C$ values in drippings and stalagmites [33,34]. (2) During the dry season or climate dry periods, the lower precipitation and soil $CO_2$ concentration lead to positive $\delta^{13}C$ values, signifying a preferential deposition of calcium carbonate in the aquifer, extended degassing periods, and slightly positive $\delta^{13}C$ values in drippings and stalagmites [36]. These observations reflect the dynamic responses of speleothem $\delta^{13}C$ records to climatic and environmental changes in the region.

### 3.3. Interpretation of the Trace Element Records

Previous research has demonstrated that the ratios of Mg/Ca and Sr/Ca are sensitive to fluctuations in local rainfall and the intensity of regional monsoons [37]. The element/Ca ratios in stalagmites serve as proxies for rainfall and water infiltration within the cave system, given that elements present in drip water are ultimately incorporated into calcite deposits [35,38–40]. Specifically, the element/Ca values of the drip water in the epikarst are influenced by the water–rock interaction (WRI), prior calcite precipitation (PCP), and incongruent calcite dissolution (ICD) [35,38–40]. PCP tends to reduce $Ca^{2+}$ concentrations in drip water, while ICD results in a disproportionate dissolution of $Mg^{2+}$ and $Sr^{2+}$ relative to $Ca^{2+}$, leading to elevated element/Ca ratios in both drip water and subsequently in speleothems [41]. Typically, drier climate conditions enhance $pCO_2$ degassing—either within the cave or in gas-filled voids in the host rock above the cave—leading to increased PCP, higher $\delta^{13}C$ values, and elevated Mg/Ca (and potentially Sr/Ca) ratios in drip water and stalagmites. Conversely, wetter conditions are associated with reduced $pCO_2$ degassing, decreased PCP, lower $\delta^{13}C$ values, and diminished Mg/Ca ratios [42,43].

## 4. Discussion

### 4.1. Temporospatial Patterns of Climate in Southern Thailand

The $\delta^{18}O$ ($\delta^{13}C$) values of the TNL3 record are relatively stable with an amplitude of variation of ~3‰ (4‰), from −7.5 to −4.5‰ (−11.5 to −7.5‰) (Figure 4). Our speleothem $\delta^{18}O$ and the Mg/Ca records (Figure 4) suggest that precipitation in Southern Thailand remains relatively stable under current warming trends, in contrast to the significant droughts or humidity observed in other regions [10,44]. This discrepancy emphasizes the varied regional precipitation responses to the temperature changes or may highlight the unique precipitation dynamics in tropical areas.
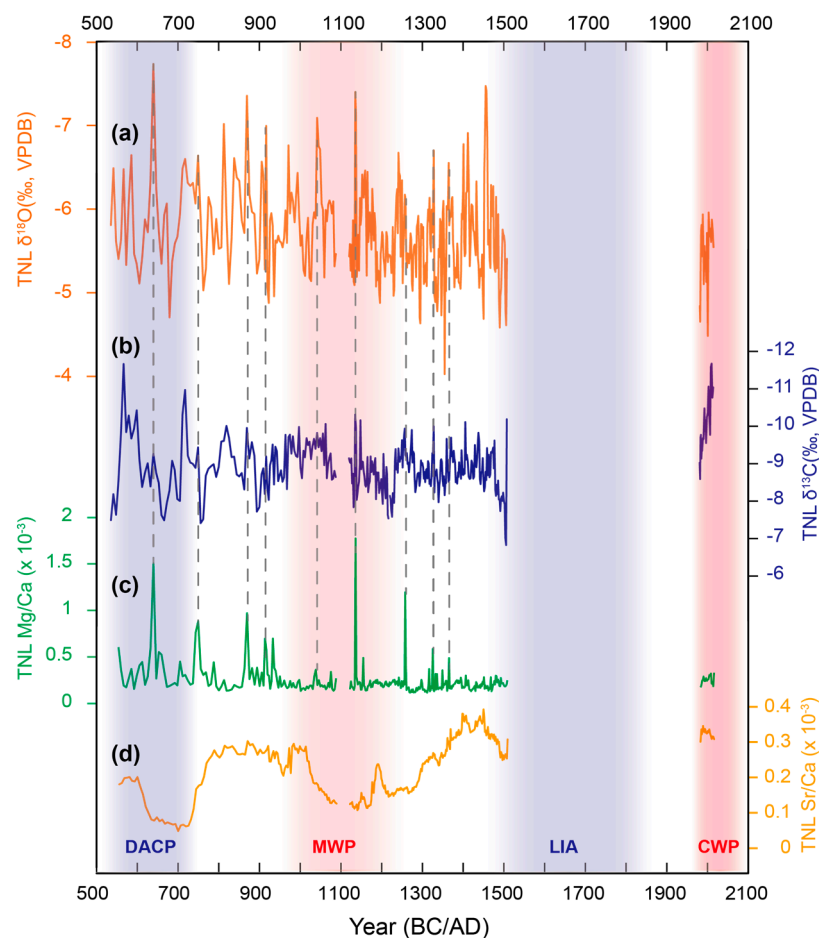
**Figure 4.** TNL3 $\delta^{18}$O, $\delta^{13}$C, and elements/Ca. From top to bottom: (**a**) $\delta^{18}$O, (**b**) $\delta^{13}$C, (**c**) Mg/Ca, (**d**) Sr/Ca. The blue and red bars depict typical cold (Dark Ages Cold Period and Little Ice Age) and warm (Medieval Warm Period and Current Warm Period) periods. Grey dashed lines mark the peaks of $\delta^{18}$O (**a**) and Mg/Ca (**c**), which might be indicators of heavy rainfall events.

On multi-centennial scales, our TNL3 $\delta^{18}$O, $\delta^{13}$C, and Mg/Ca records do not show the features of typical cold and warm periods (Figure 4), such as the Dark Ages Cold Period (DACP) and Medieval Warm Period (MWP), except for the hiatus during the Little Ice Age (LIA) and abrupt changes in speleothem $\delta^{13}$C during the Current Warm Period (CWP). In contrast, previously published speleothem records from Southern Thailand [11] display distinct responses to these climatic fluctuations. This divergence may stem from differences in tropical rainfall patterns or the influence of topography on local climate conditions (Figure 1a).

Indeed, our speleothem $\delta^{18}$O, $\delta^{13}$C, and Mg/Ca records display consistent short-term fluctuations, marked by peaks that are indicative of heavy rainfall events or changes in cave ventilation. One reason for these patterns is the influence of rainfall and cave air pCO$_2$ levels on WRI and PCP, which subsequently affect the variations in Mg/Ca and $\delta^{13}$C [45]. Additionally, changes in petrography impact the ratios of trace elements in stalagmites. Instabilities in the geochemical properties of cave drip water, along with shifts in mineralogy from aragonite to calcite on stalagmite surfaces, lead to significant increases in the Mg/Ca ratio of the calcium carbonate [46]. Although the solution properties of these minerals are similar, the Mg/Ca ratio in calcite is higher than in aragonite [46]. This phenomenon is evidenced in our stalagmite TNL3 profile, which features multiple gray bands where increased Mg/Ca ratios are observed (Figure 2). Conversely, the speleothem Sr/Ca ratio exhibits a trend that diverges from other indicators, possibly because the Sr partition coefficient is affected by the growth rate of calcium carbonate which has

been demonstrated by experimental studies [47]. However, the growth rate is not the predominant factor influencing the variation in Sr/Ca ratios. Instead, the distribution coefficients for Mg and Sr, which are controlled by temperature, precipitation rate, and pH, remain variable [48,49]. Therefore, attributing the centennial cyclical patterns observed in Sr/Ca ratios directly to climatic signals is challenging and necessitates further research.

*4.2. Influence of the ENSO on Precipitation in Southern Thailand*

The climate over southern Thailand is closely linked to the atmospheric and oceanic dynamics in the Pacific sector (Figures 1d and 3b). Within modern climatology, moisture convergence in the study area varies inter-annually in association with El Niño Southern Oscillation (ENSO), as more (less) evaporated water originating from the Pacific Ocean converges over southern Thailand with a strengthened (depressed) Walker Circulation during La Niña (El Niño) mode (Figure 3b), accompanied by high precipitation during La Niña and vice versa during El Niño in southern Thailand (Figure 3b).

The previous study suggests that the multi-decadal periods of extreme ENSO behavior could occur by chance, underscoring an unpredictable nature [50]. Climate simulations support this view, suggesting that multi-decadal fluctuations in the ENSO variability in the tropical Pacific Ocean may be inherently unpredictable [51]. Nevertheless, the ENSO reconstruction, derived from the North American Drought Atlas—a collection of drought reconstructions based on tree ring data—employs Empirical Orthogonal Function (EOF) analysis to isolate the dominant mode of the data [52], revealing substantial multi-decadal variability (Figure 5b). The comparison of our speleothem $\delta^{18}O$ record from southern Thailand and the ENSO reconstruction shows notable consistency (Figure 5a,b). Positive ENSO variability coincides with wetter conditions, revealed by our speleothem $\delta^{18}O$ record, indicating that the ENSO variability is associated with hydroclimate conditions in southern Thailand [11,53]. This observation suggests that the speleothem $\delta^{18}O$ record could provide valuable insights into reconstructing the variability of ENSO on multi-decadal scales.
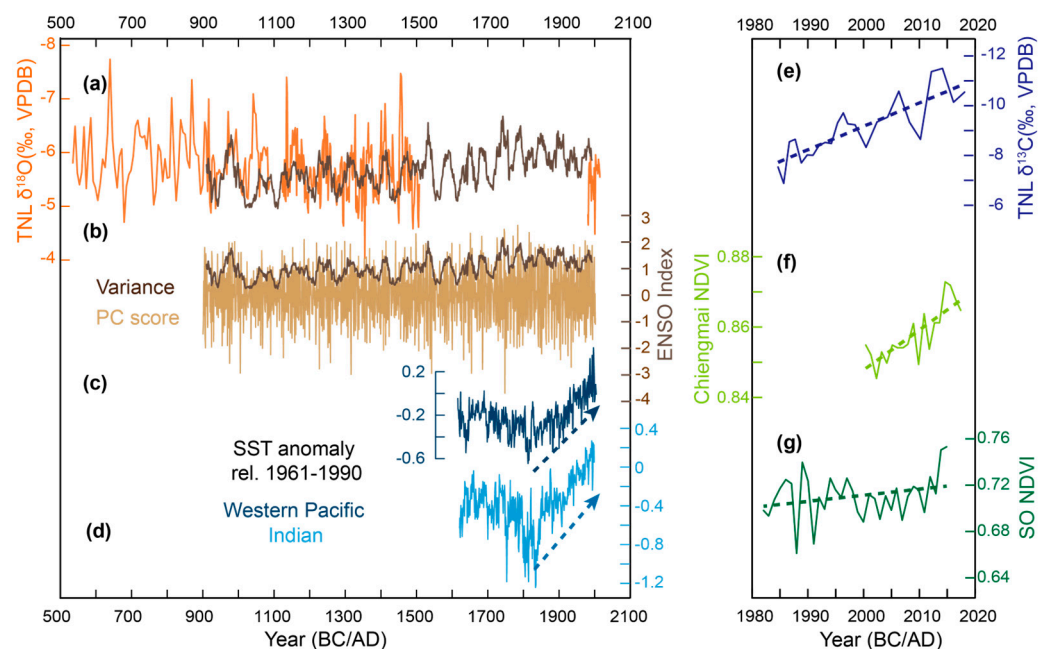


**Figure 5.** The comparison between TNL records and ENSO, sea surface temperature (SST), and Normalized Difference Vegetation Index (NDVI). (**a**) TNL $\delta^{18}O$ and the ENSO variance (dark brown, same as (**b**)). (**b**) The annual ENSO index (light brown) reconstructed from the North American Drought Atlas [52], and the amplitude variance (dark brown). The SST anomaly relative to 1961–1990 in the western Pacific (**c**) and Indian oceans (**d**), respectively [54]. (**e**) TNL $\delta^{13}C$ record. (**f**) The inter-annual NDVI from Chiengmai [55]. (**g**) The seasonal NDVI for September and October [55]. The dashed lines show the linear trend.

For the impact on precipitation in the Indo-Pacific, the ENSO's influence is relatively indirect, with a more direct effect stemming from changes in ocean and land surface circulation caused by abnormal heat sources in the Indian Ocean. The potential mechanism underlying the reflection of ENSO variability in our speleothem $\delta^{18}$O record appears to be located at the intersection of the Indian Ocean Dipole (IOD) and ENSO. This critical juncture is marked by regular oscillations between the La Niña and El Niño states, or absolute changes that can alter local sea surface temperatures (Figure 5c,d) or cause extensive atmospheric circulation patterns [53]. Such fluctuations are capable of affecting local rainfall patterns, with a tendency for reduced rainfall during periods of comparative stability.

### *4.3. Vegetation Greenness in Response to Climate Change in Southern Thailand*

Our speleothem $\delta^{13}$C shows an abrupt decrease of ~2‰, which corresponds to an increasing trend in NDVI values for both deciduous and evergreen forests from 1982 to 2015 (Figure 5f,g). Based on the analysis of vegetation change and its response to climate change in the Indo-Pacific from 1982 to 2015, the results show that there are significant inter-annual changes in vegetation cover, with spring and autumn being the most significant seasons for vegetation growth [56,57]. In Northeast Thailand, the high-value areas of NDVI correspond to vegetation types, mainly broad-leaved forests, coniferous forests, and mixed forests [16,58]. From its intergenerational changes, vegetation has shown a trend of greening in the past thirty years, mainly due to the increase in farmland caused by human activities [59]. For example, land use in southern Thailand changed significantly after the 16th century, with large-scale plantations of rubber and pepper replacing the original tropical rainforests and wetlands [60], and therefore, regional social factors may be important in influencing the greenness of vegetation in southern Thailand.

Indeed, the study from Northeast Thailand indicated that the NDVI in dry evergreen forests was correlated with temperature, and overall productivity in dry evergreen forests was affected by increasing temperatures [16,58]. It is noteworthy that the rapid increase in NDVI values in southern Thailand (Figure 5) coincides with the rise in anthropogenic atmospheric $CO_2$ levels [61]. The climate change induced by greenhouse gas forcing may be responsible for the rapid development of the increased trend in NDVI in southern Thailand during the past thirty years, and thus, this anthropogenic signal was recorded in our speleothems $\delta^{13}$C.

Moreover, global warming cannot cause vegetation changes directly, as climate change in southern Thailand is the result of interactions between energy and hydrological cycles. The increase in sea surface temperature is the same as the pattern with our speleothem $\delta^{13}$C and NDVI (Figure 5f,g), suggesting that when the sea surface temperature in the western Pacific and the Indian Ocean rises (Figure 5c,d), the growth ability of vegetation increases. The reason is that sea surface temperature can affect the growth of vegetation in the Indo-Pacific through atmospheric circulation [62]. The increase in sea surface temperature leads to an increase in precipitation in the Indo-Pacific, which is conducive to vegetation growth.

### 5. Conclusions

The investigation of climate variability across various temporal scales—from centuries and decades to inter-annual periods—is crucial for comprehending the intricate relationship between human activities and climate change. It aids in discerning the natural backdrop against which modern and future climate shifts occur, thereby enabling predictions and the implementation of appropriate response strategies. To enhance our comprehension of climate and vegetation change dynamics in southern Thailand, we have reconstructed and extensively analyzed multiple proxy speleothem records covering the past 1500 years, excluding the hiatus during the Little Ice Age. Our analysis underscores a pronounced correlation between speleothem $\delta^{18}$O values and ENSO variability, providing a reference for the historical reconstruction of ENSO's long-term fluctuations, thereby enriching our understanding of ENSO's multi-decadal fluctuations. Additionally, a comparison of the carbon isotopes and Normalized Difference Vegetation Index (NDVI) data from recent

decades indicates a marked influence of climate change on vegetation dynamics, highlighting the intricate nexus between climatic shifts and ecosystem dynamics. Notably, even among proximate regions, our findings reveal substantial disparities in climate records across various temporal scales. These discrepancies may reflect the diversity in tropical precipitation patterns or the impact of topographical features. Overall, our research contributes valuable empirical data and perspectives on the climatic transformations in Thailand's southern territories, offering a foundation for future research in climate change and bolstering environmental conservation initiatives.

**Supplementary Materials:** The following supporting information can be downloaded at https://www.mdpi.com/article/10.3390/min14050519/s1, Table S1: TNL3 U-Th dating results; Table S2: TNL3 Age model and proxies.

**Conflicts of Interest:** The authors declare no conflicts of interest.

# References

1. Trenberth, K.E.; Dai, A.; Van Der Schrier, G.; Jones, P.D.; Barichivich, J.; Briffa, K.R.; Sheffield, J. Global warming and changes in drought. *Nat. Clim. Chang.* **2014**, *4*, 17–22. [CrossRef]
2. Monastersky, R. Anthropocene: The human age. *Nature* **2015**, *519*, 144–147. [CrossRef] [PubMed]
3. Subramanian, M. Humans versus Earth: The quest to define the Anthropocene. *Nature* **2019**, *572*, 168–170. [CrossRef] [PubMed]
4. Jones, P.D.; Briffa, K.R.; Osborn, T.J.; Lough, J.M.; Van Ommen, T.D.; Vinther, B.M.; Luterbacher, J.; Wahl, E.R.; Zwiers, F.W.; Mann, M.E.; et al. High-resolution palaeoclimatology of the last millennium: A review of current status and future prospects. *Holocene* **2009**, *19*, 3–49. [CrossRef]
5. Loehle, C. A 2000-year global temperature reconstruction based on non-tree ring proxies. *Energy Environ.* **2007**, *18*, 1049–1058. [CrossRef]
6. IPCC. *Climate Change 2021: The Physical Science Basis*; Cambridge University Press: Cambridge, UK; New York, NY, USA, 2021; pp. 33–144. [CrossRef]
7. PAGES. *Science Plan and Implementation Strategy (IGBP Report No.57)*; IGBP Secretariat: Stockholm, Sweden, 2009; pp. 1–67. Available online: http://www.igbp.net/publications/reportsandscienceplans/reportsandscienceplans/reportno57.5.1b8ae205 12db692f2a680006621.html (accessed on 5 November 2023).
8. Stone, D.A.; Allen, M.R.; Stott, P.A.; Pall, P.; Min, S.-K.; Nozawa, T.; Yukimoto, S. The detection and attribution of human influence on climate. *Ann. Rev. Environ. Resource* **2009**, *34*, 1–16. [CrossRef]
9. Sha, L.; Ait Brahim, Y.; Wassenburg, J.A.; Yin, J.; Peros, M.; Cruz, F.W.; Cai, Y.; Li, H.; Du, W.; Zhang, H.; et al. How far north did the African Monsoon fringe expand during the African Humid Period?—Insights from Southwest Moroccan speleothems. *Geophys. Res. Lett.* **2019**, *46*, 14093–14102. [CrossRef]
10. Sha, L.; Ait Brahim, Y.; Wassenburg, J.A.; Yin, J.; Lu, J.; Cruz, F.W.; Cai, Y.; Edwards, R.L.; Cheng, H. The "Hockey Stick" Imprint in Northwest African Speleothems. *Geophys. Res. Lett.* **2021**, *48*, e2021GL094232. [CrossRef]
11. Tan, L.; Shen, C.-C.; Löwemark, L.; Chawchai, S.; Edwards, R.L.; Cai, Y.; Breitenbach, S.F.M.; Cheng, H.; Chou, Y.-C.; Duerrast, H.; et al. Rainfall variations in central Indo-Pacific over the past 2700 y. *Proc. Natl. Acad. Sci. USA* **2019**, *116*, 17201–17206. [CrossRef]
12. Yin, J.; Xu, Q.; Siripornpibul, C.; Siripattarapureenon, R.; Wu, X.; Tang, W.; Cheng, H.; Ning, Y.; Qin, Z. Hydroclimate variability in early stage of late Holocene recorded by stalagmite from Southern Thailand. *Carsol. Sin.* **2023**, *42*, 573–581. Available online: http://en.cgsjournals.com/article/doi/10.11932/karst20230307?viewType=HTML (accessed on 5 November 2023). (In Chinese)

13.  Cai, B.G.; Pumijumnong, N.; Tan, M. Effects of intraseasonal variation of summer monsoon rainfall on stable isotope and growth rate of a stalagmite from northwestern Thailand. *J. Geophys. Res.* **2010**, *115*, D21104. [CrossRef]

14.  Chawchai, S.; Chabangborn, A.; Fritz, S.; Väliranta, M.; Mörth, C.M.; Blaauw, M.; Reimer, P.J.; Krusic, P.J.; Löwemark, L.; Wohlfarth, B. Hydroclimatic shifts in Northeast Thailand during the last two millennia: The record of Lake Pa Kho. *Quat. Sci. Rev.* **2015**, *111*, 62–71. [CrossRef]

15.  Cheng, H.; Zhang, H.; Cai, Y.; Shi, Z.; Yi, L.; Deng, C.; Hao, Q.; Peng, Y.; Sinha, A.; Li, H.; et al. Orbital-scale Asian summer monsoon variations: Paradox and exploration. *Sci. China Earth Sci.* **2021**, *63*, 529–544. [CrossRef]

16.  Maxwell, J.F. A synopsis of the vegetation of Thailand. *Nat. Hist. J. Chulalongkorn Univ.* **2004**, *4*, 19–29. Available online: https://www.thaiscience.info/Journals/Article/NHCU/10439727.pdf (accessed on 10 November 2023).

17.  du Plessis, W.P. Linear regression relationship between NDVI vegetation and rainfall in Etosha National Park, Namibia. *J. Arid Environ.* **1999**, *42*, 235–260. [CrossRef]

18.  Pettorellii, N.; Vik, J.O.; Mysterud, A.; Gaillard, J.-M.; Tucker, C.J.; Stenseth, N.C. Using the satellite-derived NDVI to assess ecological response to environmental change. *Trends Ecol. Evol.* **2005**, *20*, 503–510. [CrossRef] [PubMed]

19.  Seneviratne, S.I.; Corti, T.; Davin, E.L.; Hirschi, M.; Jaeger, E.B.; Lehner, I.; Orlowsky, B.; Teuling, A.J. Investigating soil moisture-climate interactions in a changing climate: A review. *Earth Sci. Rev.* **2010**, *99*, 125–161. [CrossRef]

20.  Pielke, R.A.; Pitman, A.; Niyogi, D.; Mahmood, R.; McAlpine, C.; Hossain, F.; Goldewijk, K.K.; Nair, U.; Betts, R.; Fall, S.; et al. Land use/land cover changes and climatic: Modeling analysis and observational evidence. *WIREs Clim. Chang.* **2011**, *2*, 828–850. [CrossRef]

21.  Sha, L.; Wassenburg, J.A.; Sha, L.; Li, Y.; Zhou, S.; Liang, Q.; Zhao, J.; Ruan, J.; Li, H.; Zhao, X.; et al. Variations in triple oxygen isotope of speleothems from the Asian monsoon region reveal moisture sources over the past 300 years. *Commun. Earth Environ.* **2023**, *4*, 384. [CrossRef]

22.  Chen, Z.; Auler, A.S.; Bakalowicz, M.; Drew, D.; Griger, F.; Hartmann, J.; Jiang, G.; Moosdorf, N.; Richts, A.; Stevanovic, Z.; et al. The World Karst Aquifer Mapping project: Concept, mapping procedure and map of Europe. *Hydrogeol. J.* **2017**, *25*, 771–785. [CrossRef]

23.  Kalnay, E.; Kanamitsu, M.; Kistler, R.; Collins, W.; Deaven, D.; Gandin, L.; Iredell, M.; Saha, S.; White, G.; Woollen, J.; et al. The NCEP/NCAR 40-Year Reanalysis Project. *Bull. Am. Meteorol. Soc.* **1996**, *77*, 437–471. [CrossRef]

24.  Edwards, R.L.; Chen, J.H.; Wasserburg, G.J. $^{238}$U, $^{234}$U, $^{230}$Th, $^{232}$Th systematics and the precise measurement of time over the past 500,000 years. *Earth Planet. Sci. Lett.* **1987**, *81*, 175–192. [CrossRef]

25.  Cheng, H.; Edwards, R.L.; Shen, C.-C.; Polyak, V.J.; Asmerom, Y.; Woodhead, J.; Hellstrom, J.; Alexander, E.C., Jr. Improvements in $^{230}$Th dating, $^{230}$Th and $^{234}$U half-life values, and U–Th isotopic measurements by multi-collector inductively coupled plasma mass spectrometry. *Earth Planet. Sci. Lett.* **2013**, *371–372*, 82–91. [CrossRef]

26.  Hercman, H.; Pawlak, J. MOD-AGE: An age-depth model construction algorithm. *Quat. Geochronol.* **2012**, *12*, 1–10. [CrossRef]

27.  Breitenbach, S.F.M.; Rehfeld, K.; Goswami, B.; Baldini, J.U.L.; Ridley, H.E.; Kennett, D.J. Constructing Proxy Records from Age models (COPRA). *Clim. Past.* **2012**, *8*, 1765–1779. [CrossRef]

28.  Scholz, D.; Hoffmann, D.L. StalAge—An algorithm designed for construction of speleothem age models. *Quat. Int.* **2011**, *6*, 369–382. [CrossRef]

29.  Wei, Z.; Lee, X.; Liu, Z.; Seeboonruang, U.; Koike, M.; Yoshimura, K. Influences of large-scale convection and moisture source on monthly precipitation isotope ratios observed in Thailand, Southeast Asia. *Earth Planet. Sci. Lett.* **2018**, *488*, 181–192. [CrossRef]

30.  Adler, R.F.; Huffman, G.J.; Chang, A.; Ferraro, R.; Xie, P.-P.; Janowiak, J.; Rudolf, B.; Schneider, U.; Curtis, S.; Bolvin, D.; et al. The version 2 Global Precipitation Climatology Project (GPCP) Monthly Precipitation Analysis (1979-present). *J. Hydrometeor.* **2003**, *4*, 1147–1167. [CrossRef]

31.  Fohlmeister, J.; Voarintsoa, N.R.G.; Lechleitner, F.A.; Boyd, M.; Brandtsta¨tter, S.; Jacobson, M.J.; Oster, J.L. Main controls on the stable carbon isotope composition of speleothems. *Geochim. Cosmochim. Acta.* **2020**, *279*, 67–87. [CrossRef]

32.  Martín-Chivelet, J.; Muñoz-García, M.B.; Edwards, R.L.; Turrero, M.J.; Ortega, A.I. Land surface temperature changes in Northern Iberia since 4000 yr BP, based on $\delta^{13}$C of speleothems. *Glob. Planet. Chang.* **2011**, *77*, 1–12. [CrossRef]

33.  Dorale, J.A.; Edwards, R.L.; Ito, E.; González, L.A. Climate and Vegetation History of the Midcontinent from 75 to 25 ka: A Speleothem Record from Crevice Cave, Missouri, USA. *Science* **1998**, *282*, 1871–1874. [CrossRef] [PubMed]

34.  McDermott, F. Palaeo-climate reconstruction from stable isotope variations in speleothems: A review. *Quat. Sci. Rev.* **2004**, *23*, 901–918. [CrossRef]

35.  Johnson, K.R.; Hu, C.Y.; Belshaw, N.S.; Henderson, G.M. Seasonal trace-element and stable-isotope variations in a Chinese speleothem: The potential for high- resolution paleomonsoon reconstruction. *Earth Planet. Sci. Lett.* **2006**, *244*, 394–407. [CrossRef]

36.  Hansen, M.; Scholz, d.; Schöne, B.R.; Spötl, C. Simulating speleothem growth in the laboratory: Determination of the stable isotope fractionation ($\delta^{13}$C and $\delta^{18}$O) between $H_2O$, DIC and $CaCO_3$. *Chem. Geol.* **2019**, *509*, 20–44. [CrossRef]

37.  Owen, R.A.; Day, C.C.; Hu, C.-Y.; Liu, Y.-H.; Pointing, M.D.; Blättler, C.L.; Henderson, G.M. Calcium isotopes in caves as a proxy for aridity: Modern calibration and application to the 8.2 kyr event. *Earth Planet. Sci. Lett.* **2016**, *443*, 129–138. [CrossRef]

38.  McDonald, J.; Drysdale, R.; Hill, D.; Chisari, R.; Wong, H. The hydrochemical response of cave drip waters to sub-annual and inter-annual climate variability, Wombeyan Caves, SE Australia. *Chem. Geol.* **2007**, *244*, 605–623. [CrossRef]

39.  Oster, J.L.; Montañez, I.P.; Kelley, N.P. Response of a modern cave system to large seasonal precipitation variability. *Geochim. Cosmochim. Acta* **2012**, *91*, 92–108. [CrossRef]

40. Zhang, J.; Li, T.-Y. Seasonal and interannual variations of hydrochemical characteristics and stable isotopic compositions of drip waters in Furong Cave, Southwest China based on 12 years' monitoring. *J. Hydrol.* **2019**, *572*, 40–50. [CrossRef]

41. McMillan, M.R.; Fairchild, I.J. An experimental study of incongruent dissolution of $CaCO_3$ under analogue glacial conditions. *J. Glaciol.* **2005**, *51*, 383–390. [CrossRef]

42. Fairchild, I.J.; Borsato, A.; Tooth, A.F.; Frisia, S.; Hawkesworth, C.J.; Huang, Y.M.; McDermott, F.; Spiro, B. Controls on trace element (Sr–Mg) compositions of carbonate cave waters: Implications for speleothem climatic records. *Chem. Geol.* **2000**, *166*, 255–269. [CrossRef]

43. Fairchild, I.J.; Treble, P.C. Trace elements in speleothems as recorders of environmental change. *Quat. Sci. Rev.* **2009**, *28*, 449–468. [CrossRef]

44. Stríkis, N.M.; Buarque, P.F.S.M.; Cruz, F.W.; Bernal, J.P.; Vuille, M.; Tejedor, E.; Santos, S.; Shimizu, M.H.; Ampuero, A.; Du, W.; et al. Modern anthropogenic drought in Central Brazil unprecedented during last 700 years. *Nat. Commun.* **2024**, *15*, 1728. [CrossRef] [PubMed]

45. Lyu, Y.; Luo, W.; Wang, Y.; Zeng, G.; Chen, J.; Wang, S. Response of drip water Mg/Ca and Sr/Ca variations in ventilated caves to hydroclimate. *Sci. Total Environ.* **2023**, *874*, 162626. [CrossRef] [PubMed]

46. Hashim, M.S.; Kaczmarek, S.E. The transformation of aragonite to calcite in the presence of magnesium: Implications for marine diagenesis. *Earth Planet. Sci. Lett.* **2021**, *574*, 117166. [CrossRef]

47. Li, J.-Y.; Li, T.-Y.; Shen, C.-C.; Yu, T.-L.; Zhang, T.-T.; Wu, Y.; Zhou, J.-L.; Chen, C.-J.; Zhang, J. Variations and significance of Mg/Sr and $^{87}Sr/^{86}Sr$ in a karst cave system in southwest China. *J. Hydrol.* **2021**, *596*, 126140. [CrossRef]

48. Day, C.C.; Henderson, G.M. Controls on trace-element partitioning in cave-analogue calcite. *Geochim. Cosmochim. Acta* **2013**, *120*, 612–627. [CrossRef]

49. Gabitov, R.I.; Sadekov, A.; Leinweber, A. Crystal growth rate effect on Mg/Ca and Sr/ Ca partitioning between calcite and fluid: An in situ approach. *Chem. Geol.* **2014**, *367*, 70–82. [CrossRef]

50. Wittenberg, A.T.; Rosati, A.; Delworth, T.L.; Vecchi, G.A.; Zeng, F. ENSO Modulation: Is It Decadally Predictable? *J. Clim.* **2014**, *27*, 2667–2681. [CrossRef]

51. DiNezio, P. A high bar for decadal forecasts of El Niño. *Nature* **2014**, *507*, 437–439. [CrossRef]

52. Li, J.; Xie, S.-P.; Cook, E.R.; Huang, G.; D'Arrigo, R.; Liu, F.; Ma, J.; Zheng, X.-T. Interdecadal modulation of El Niño amplitude during the past millennium. *Nat. Clim. Chang.* **2011**, *1*, 114–118. [CrossRef]

53. Muangsong, C.; Cai, B.; Pumijumnong, N.; Hu, C.; Cheng, H. An annually laminated stalagmite record of the changes in Thailand monsoon rainfall over the past 387 years and its relationship to IOD and ENSO. *Quat. Int.* **2014**, *349*, 90–97. [CrossRef]

54. Tierney, J.E.; Abram, N.J.; Anchukaitis, K.J.; Evans, M.N.; Giry, C.; Kilbourne, K.H.; Saenger, C.P.; Wu, H.C.; Zinke, J. Tropical sea surface temperatures for the past four centuries reconstructed from coral archives. *Paleoceanography* **2015**, *30*, 226–252. [CrossRef]

55. Chen, H.S.; Qian, M.Y.; Hua, W.J. Vegetation cover change in the Indo-China Peninsula in spring and its relation to ENSO. *Trans. Atmos. Sci.* **2020**, *43*, 1065–1075. [CrossRef]

56. Heaney, L.R. A Synopsis of Climatic and Vegetational Change in Southeast Asia. *Clim Chang.* **1991**, *19*, 53–61. [CrossRef]

57. Stibig, H.-J.; Achard, F.; Carboni, S.; Raši, R.; Miettinen, J. Change in tropical forest cover of Southeast Asia from 1990 to 2010. *Biogeosciences* **2014**, *11*, 47–258. [CrossRef]

58. Thavorntam, W.; Tantemsapya, N. Vegetation greenness modeling in response to climate change for Northeast Thailand. *J. Geogr. Sci.* **2013**, *23*, 1052–1068. [CrossRef]

59. Lawrence, D.; Vandecar, K. Effects of tropical deforestation on climate and agriculture. *Nat. Clim. Chang.* **2015**, *5*, 27–36. [CrossRef]

60. Liang, Z.M.; Li, M.; Yang, B.J. *Ancient History of Southeast Asia—Upper Antiquity to the Early 16th Century*; Peking University Press: Beijing, China, 2013; pp. 289–312.

61. IPCC. *Climate Change 2007: The Physical Science Basis*; Cambridge University Press: Cambridge, UK; New York, NY, USA, 2007; pp. 21–64. Available online: https://www.ipcc.ch/report/ar4/wg1/ (accessed on 15 November 2023).

62. Buckley, B.M.; Palakit, K.; Duangsathaporn, K.; Sanguantham, P.; Prasomsin, P. Decadal scale droughts over northwestern Thailand over the past 448 years: Links to the tropical Pacific and Indian Ocean sectors. *Clim. Dyn.* **2007**, *29*, 63–71. [CrossRef]